

Nano-mechanical tuning and imaging of a photonic crystal micro-cavity resonance

W. C. L. Hopman, A. J. F. Hollink, and R. M. de Ridder

Faculty of Electrical Engineering, Mathematics and Computer Science, Mesa+ Institute for Nanotechnology,
University of Twente, PO Box 217, 7500AE Enschede, The Netherlands
Wico.Hopman@utwente.nl, R.M.deRidder@ewi.utwente.nl

K. O. van der Werf, and V. Subramaniam

Faculty of Science and Technology, Mesa+ Institute for Nanotechnology, University of Twente, PO Box 217, 7500AE
Enschede, The Netherlands
K.O.vanderWerf@tmw.utwente.nl, V.Subramaniam@tmw.utwente.nl

W. Bogaerts

Department of Information Technology, Ghent University – IMEC, Sint-Pietersnieuwstraat 41, 9000 Gent, Belgium
Wim.Bogaerts@ugent.be

Abstract: We show that nano-mechanical interaction using atomic force microscopy (AFM) can be used to map out mode-patterns of an optical micro-resonator with high spatial accuracy. Furthermore we demonstrate how the Q-factor and center wavelength of such resonances can be sensitively modified by both horizontal and vertical displacement of an AFM tip consisting of either Si₃N₄ or Si material. With a silicon tip we are able to tune the resonance wavelength by 2.3 nm, and to set Q between values of 615 and zero, by expedient positioning of the AFM tip. We find full on/off switching for less than 100 nm vertical, and for 500 nm lateral displacement at the strongest resonance antinode locations.

©2006 Optical Society of America

OCIS codes: (230.5750) Resonators; (230.3990) Microstructure devices; (120.5820) Scattering measurements; (120.7000) Transmission; (130.3120) Integrated optics devices; (170.4520) Optical confinement and manipulation; (180.5810) Scanning microscopy; (999.9999) Photonic crystals; (999.9999) Mechano-optical tuning

References and links

1. D. Gerace, and L. C. Andreani, "Effects of disorder on propagation losses and cavity Q-factors in photonic crystal slabs," *Photon. Nanostruct.* **3**, 120-128 (2005).
2. R. Ferrini D. Leuenberger, R. Houdré, H. Benisty, M. Kamp, and A. Forchel, "Disorder-induced losses in planar photonic crystals," *Opt. Lett.* **31**, 1426-1428 (2006).
3. M. Settle, M. Salib, A. Michaeli, and T. F. Krauss, "Low loss silicon on insulator photonic crystal waveguides made by 193nm optical lithography," *Opt. Express* **14**, 2440-2445 (2006).
4. H. M. H. Chong, and R. M. De La Rue, "Tuning of photonic crystal waveguide microcavity by thermo-optic effect," *IEEE Photon. Technol. Lett.* **16**, 1528-1530 (2004).
5. Y. A. Vlasov, M. O'Boyle, H. F. Hamann, and S. J. McNab, "Active control of slow light on a chip with photonic crystal waveguides," *Nature* **438**, 65-69 (2005).
6. W. C. L. Hopman, P. Pottier, D. Yudistira, J. van Lith, P. V. Lambeck, R. M. De La Rue, A. Driessen, H. J. W. M. Hoekstra, and R. M. de Ridder, "Quasi-one-dimensional photonic crystal as a compact building-block for refractometric optical sensors," *IEEE J. Sel. Top. Quantum Electron.* **11**, 11-16 (2005).
7. R. van der Heijden, C. F. Carlström, J. A. P. Snijders, R. W. van der Heijden, F. Karouta, R. Nötzel, H. W. M. Salemink, B. K. C. Kjellander, C. W. M. Bastiaansen, D. J. Broer, and E. Drift van der, "InP-based two-dimensional photonic crystals filled with polymers," *Appl. Phys. Lett.* **88**, 161112-1-3 (2006).
8. S. F. Mingaleev, M. Schillinger, D. Hermann, and K. Busch, "Tunable photonic crystal circuits: concepts and designs based on single-pore infiltration," *Opt. Lett.* **29**, 2858-2860 (2004).

9. A. F. Koenderink, R. Wuest, B. C. Buchler, S. Richter, P. Strasser, M. Kafesaki, A. Rogach, R. B. Wehrspohn, C. M. Soukoulis, D. Erni, F. Robin, H. Jackel, and V. Sandoghdar, "Near-field optics and control of photonic crystals," *Photon. Nanostruct. Fundam. Appl.* **3**, 63-74 (2005).
10. I. Marki, M. Salt, and H. P. Herzig, "Tuning the resonance of a photonic crystal microcavity with an AFM probe," *Opt. Express* **14**, 2969-2978 (2006).
11. T. Takahata, K. Hoshino, K. Matsumoto, and I. Shimoyama, "Transmittance tuning of photonic crystal reflectors using an AFM cantilever," *Sens. Actuators A* **128**, 197-201 (2006).
12. P. T. Rakich et al., "Ultrawide tuning of photonic microcavities via evanescent field perturbation," *Opt. Lett.* **31**, 1241-1243 (2006).
13. S. Wonjoo, O. Solgaard, and F. Shanhai, "Displacement sensing using evanescent tunneling between guided resonances in photonic crystal slabs," *J. Appl. Phys.* **98**, 33102-1-4 (2005).
14. G. N. Nielson et al., "Integrated wavelength-selective optical MEMS switching using ring resonator filters," *IEEE Photon. Technol. Lett.* **17**, 1190-2 (2005).
15. I. Stefanon et al., "Heterodyne detection of guided waves using a scattering-type Scanning Near-Field Optical Microscope," *Opt. Express* **13**, 5553-5564 (2005).
16. M. Notomi et al., "Optical bistable switching action of Si high-Q photonic-crystal nanocavities," *Opt. Express* **13**, 2678-2687 (2005).
17. A. F. Koenderink, M. Kafesaki, B. C. Buchler, and V. Sandoghdar, "Controlling the resonance of a photonic crystal microcavity by a near-field probe," *Phys. Rev. Lett.* **95**, 153904-1-4 (2005).
18. M. Hammer, and R. Stoffer, "PSTM/NSOM modeling by 2-D quadridirectional eigenmode expansion," *J. Lightwave Technol.* **23**, 1956-1966 (2005).
19. Y. Akahane, T. Asano, B. S. Song, and S. Noda, "High-Q photonic nanocavity in a two-dimensional photonic crystal," *Nature* **425**, 944-947 (2003).
20. M. Gnan, G. Bellanca, H. Chong, P. Bassi, and R. De La Rue, "Modelling of photonic wire Bragg gratings," *Opt. Quantum Electron.* **38**, 133-148 (2006).
21. W. Bogaerts et al., "Nanophotonic waveguides in silicon-on-insulator fabricated with CMOS technology," *J. Lightwave Technol.* **23**, 401-412 (2005).
22. K. O. Vanderwerf et al., "Compact stand-alone atomic-force microscope," *Rev. Sci. Instrum.* **64**, 2892-2897 (1993).
23. H. Gersen et al., "Real-space observation of ultraslow light in photonic crystal waveguides," *Phys. Rev. Lett.* **94** (2005).

1. Introduction

Nano-mechanical interactions with the evanescent field of photonic crystal (PhC) microcavities (MCs) enable tuning of important resonator properties such as quality-factor (Q) and resonance wavelength. The fabrication of high- Q silicon-on-insulator (SOI) based PhCs demands sophisticated nanometer-scale-precision [1-3], and has driven the search for alternative resonator tuning strategies. These include using heaters to achieve thermo-optic tuning [4, 5], and pore infiltration by liquids [6], polymers [7] or liquid crystals [8] to achieve a broad tuning range. The progress in micrometer-scale integrated optics has led to an increase in attention for mechanical tuning [9-12]. Mechano-optical interactions have been utilized in for example sensor [13] and actuator [14] applications to modulate the evanescent field. Two types of interaction can be effected, namely changing the modal amplitude through the attenuation constant (leaking or scattering of light, which can be used for scanning near-field microscopy [15]), or changing its phase through the phase constant (changing the effective refractive index). In traditional mechano-optical approaches, the size of the object placed in the evanescent field is much larger than the optical wavelength [14] to obtain a sufficiently large phase shift while avoiding strong attenuation. In this case, boundary effects causing out of plane scattering can be neglected. However, if we use a resonant cavity that provides a strongly enhanced field in a small volume (that is, a high quality factor to modal volume ratio Q/V [16]), then an object as small as 10 nm in close proximity to the resonator can strongly affect the transfer properties [17, 18]. Although the analysis of nano-mechano-optical transduction is more involved than that of the classical configuration, we demonstrate that it also offers many more opportunities for manipulation of light. We explore this manipulation experimentally in great detail using a high Q/V micro-cavity in a photonic crystal slab.

2. Design and realization

For the experiments reported here, we designed a PhC MC in SOI (220 nm device layer thickness on 1 μm buried oxide) with a triangular lattice of periodicity $a = 440$ nm and a hole radius $r = 270$ nm. We chose a relatively large cavity, designed to have a resonance near 1550 nm wavelength, and a medium Q-factor of 650 with a high finesse to have a good wavelength separation of adjacent resonances. In principle the MC could be made smaller and optimized for high Q [19], but this is not needed due to the strong interaction of the probe with the cavity resonance. The Fabry-Pérot-type cavity is defined in a W1 line-defect waveguide (1 row left out), providing optical access for transmission measurements. We calculated the resonant field distribution using a finite-difference time-domain method. Although accurate modeling requires full 3D calculations [20] and consequently high computer resources, we relied on (fast) 2D calculations, which have been qualitatively validated by a 3D calculation. The pattern shows 8 fringes with two distinct major peaks in the field amplitude within the resonator, close to the entrance and exit of the cavity [see Fig. 1(a)]. One may expect that a disturbance at these two peaks will have the largest effect on two essential resonance properties: central resonance wavelength and Q .

The structure as shown in the SEM photo in Fig. 1(b), was fabricated (at IMEC, Belgium) using a process [21] involving deep UV lithography ($\lambda = 248$ nm) and reactive ion etching. The resonance wavelength $\lambda_{r,0}$ of the fabricated cavity was measured to be 1539.25 nm.

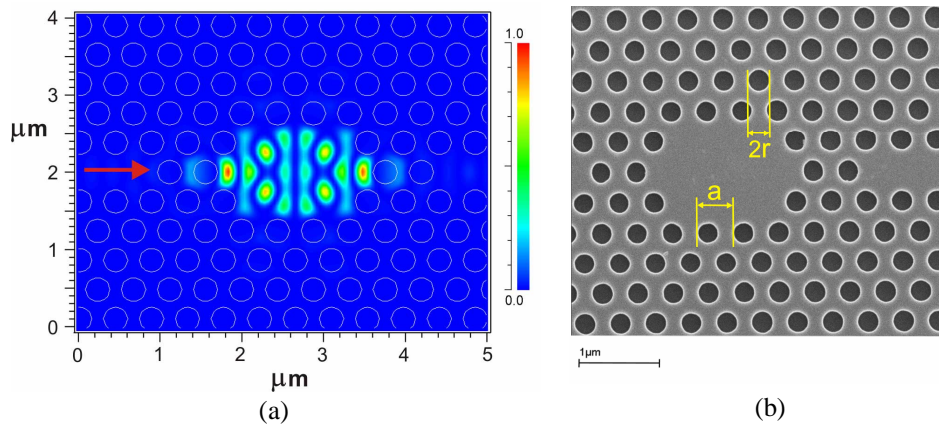


Fig. 1. Photonic crystal micro-cavity. (a) Computed optical field intensity of the resonant mode pattern. The arrow indicates the launching direction of light exciting the resonator. (b) SEM image of the micro-cavity. The period and hole radius are denoted with a and r respectively.

3. Measurement principle and imaging results

To bring a nano-sized object in the field of the resonator in a controlled way, we combined a typical optical end-fire transmission setup with a stand alone scanning tip AFM stage [22] [Fig. 2(a)]. For our first experiments we selected an AFM tip that is expected to have a relatively small impact on optical loss, by choosing a small size (minimum radius 10 nm) and a low-loss material Si_3N_4 , with a refractive index ($n_{\text{Si}_3\text{N}_4} \sim 2$) lower than the effective index of the guided mode in the photonic crystal waveguide ($n_{\text{eff}} \sim 2.9$). By raster scanning the AFM probe over the sample in contact mode and closed loop operation, we obtained both geometrical and optical transfer information from the AFM deflection data [Fig. 2(b)] and the power recorded by the photo detector [Fig. 2(c)] simultaneously. The scanning speed was kept sufficiently low to prevent artifacts caused by the limited photo detector response time. Acquisition of a typical 256×256 pixels image revealing all important details took about 45 s. We chose a 20 nm interpixel grid distance, resulting in a scanning window size of 5.2×5.2 micrometers. However, grid sizes as small as 1 nm or less can be selected when needed. By

combining both the deflection and optical transmission data, the exact locations of strong interaction of the probe with the optical field in the cavity can be visualized, as shown in Fig. 2(d), where the topographic data has been enhanced in order to improve the visibility of the holes. The figure shows how the transmitted optical power is affected by the tip through both detuning the cavity and causing scattering loss [17]. A simple intuitive model, taking into account only the tuning effect, predicts a decrease in transmitted optical power if the source wavelength λ_s is set to a value smaller than the undisturbed resonance wavelength $\lambda_{r,0}$, because the resonance wavelength λ_r is shifted further away from λ_s (to longer wavelengths). Conversely, if λ_s is longer than $\lambda_{r,0}$, an increase in transmitted power will be detected (moving up the transmission-wavelength curve of the resonance). Note, however, that this model is rather simplified, an issue addressed experimentally below.

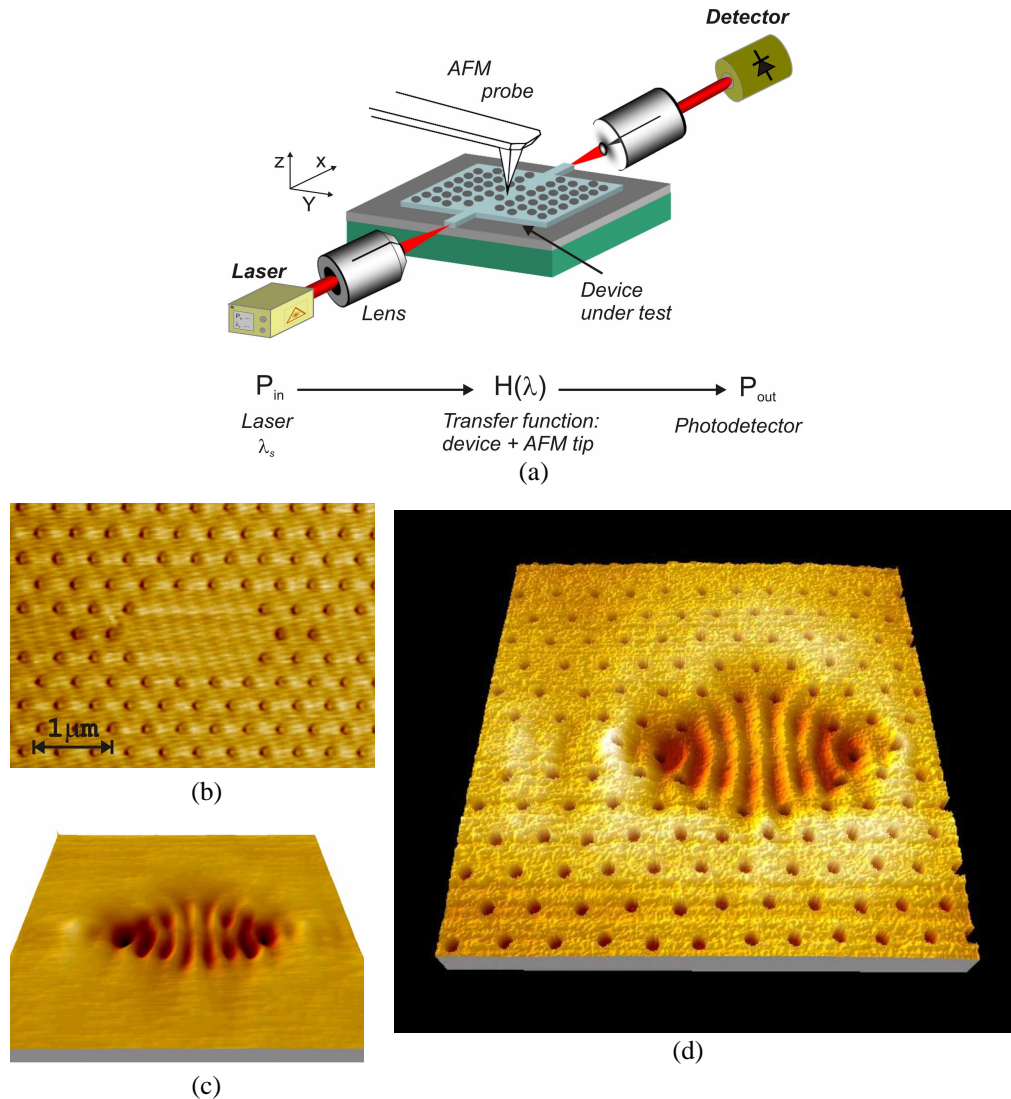


Fig. 2. Setup and optical field mapping using AFM. (a) Schematic drawing of the setup. (b) Geometry of the photonic crystal micro-cavity + input waveguide as obtained by conventional AFM probing in a raster scan. (c) Transmitted optical power recorded for each (grid) position of the scanning AFM tip. (d) Enhanced AFM image overlaying the optical detector data resulting in a precise map of the locations of maximum probe-field interaction, corresponding to amplitude peaks of the resonance pattern within the cavity.

Comparison of Figs. 2(d) and 1(a) shows that that the method can be used to find the maximum field locations of a cavity resonance. Moreover it proves that these locations are indeed the “hottest spots” for tuning [17, 18] as predicted by the simulations [Fig. 1(a)]. We have further used this innovative method of visualizing the resonator properties to study the wavelength dependent cavity disturbance. Figure 3(a) shows the transmission result for $\lambda_s = \lambda_{r,0}$ which confirms the expected decrease in power transmission at the locations of field maxima in the cavity.

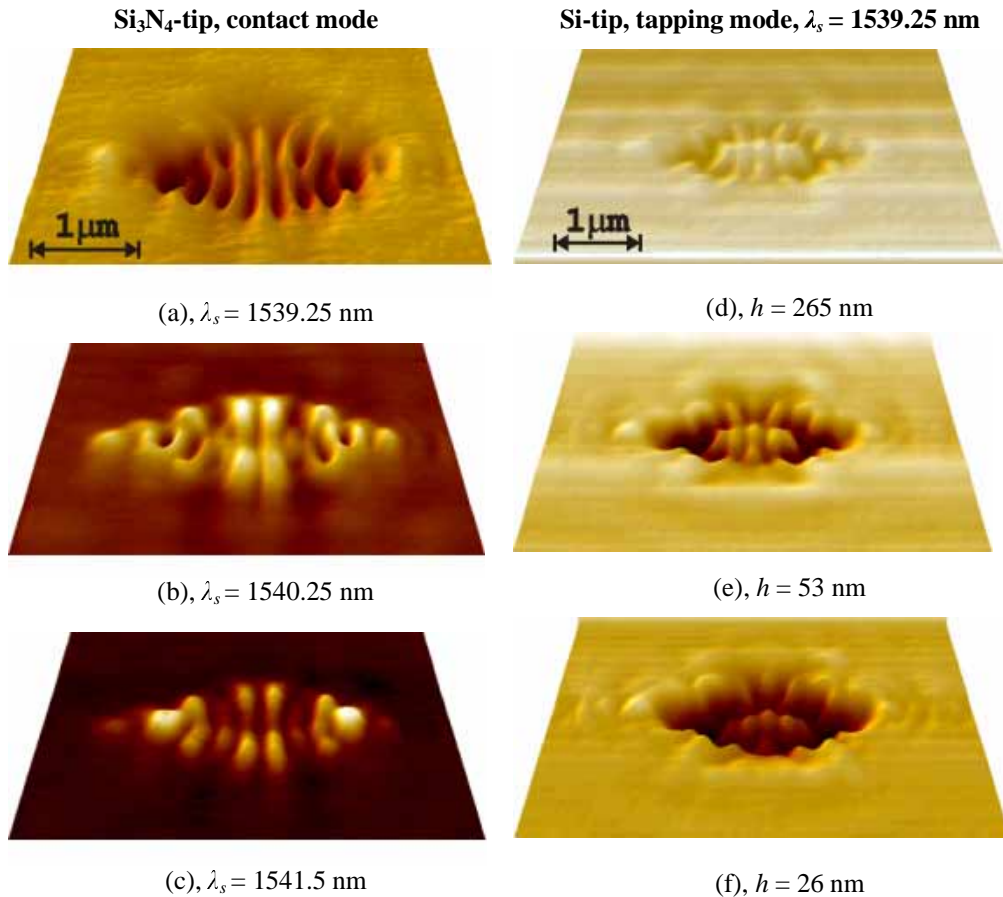
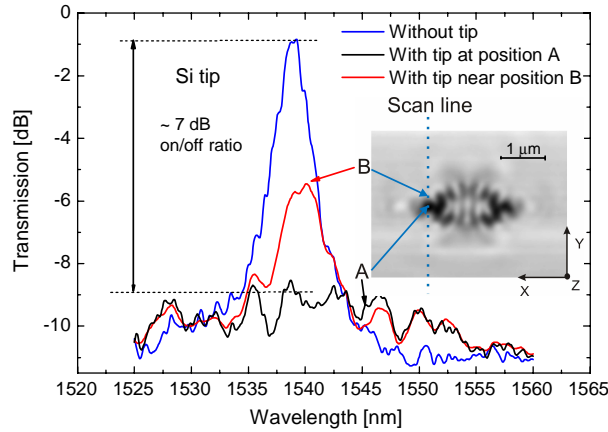


Fig. 3. Quasi 3-D representations of the position dependent probe effect on the transmission. Figs. 3(a)-3(c): Si₃N₄ probe in contact mode at different wavelengths λ_s ; Figs. 3(d)-3(f): Si tip in tapping mode with different tapping amplitudes resulting in different average probe heights (h). (a) At resonance ($\lambda_s = 1539.25$ nm $\sim \lambda_{r,0}$), showing lower transmission (dark regions) near antinodes of the optical field. (b) λ_s slightly larger than $\lambda_{r,0}$. (c) $\lambda_s \sim \lambda_{r,0}$, showing the inverse pattern of Fig. 3(a). (d) Si tip, tapping mode, large average height has small optical effect. (e), (f) Smaller average heights give larger optical effects.

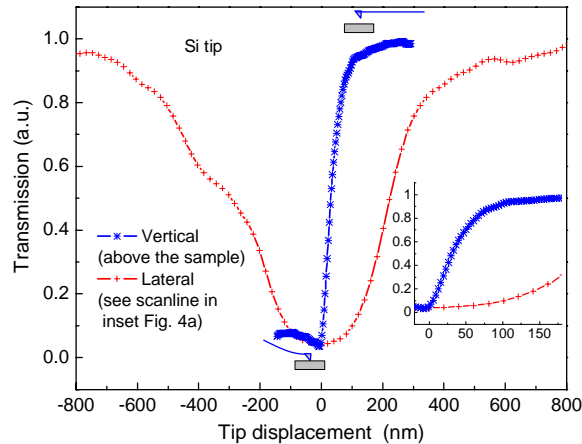
For λ_s slightly larger than $\lambda_{r,0}$ we find an interesting complex pattern, shown in Fig. 3(b), with reduced transmission at some probe locations and increased transmission at others. This complex pattern can be explained by the wavelength dependence of each extreme in the MC on the resonance wavelength shift and induced loss. Increasing λ_s further to a value larger than $\lambda_{r,0}$, we find the inverse image of Fig. 3(a), as shown in Fig. 3(c).

4. Cavity tuning method and results

A stronger response can be expected when the Si_3N_4 tip is replaced by a Si one, due to its much larger refractive index ($n_{\text{Si}} \sim 3.45$). We used a Si tip with minimum radius of only 7.5 nm. In order to explore the height dependence of the mechano-optical interaction, we used the AFM in tapping mode. By adjusting the tapping amplitude we obtained control of the average height (in time) above the surface. The very high sensitivity of transmission to the average tip height is shown in Figs. 3(d)-3(f). Another advantage of tapping mode is that the tip wears out at a much lower pace compared to contact mode.



(a)



(b)

Fig. 4. Nano-mechanical interaction. (a) Transmission spectra for the situation without probe, and with a Si probe positioned at the antinode labeled A, and at a location B close to A, as indicated in the inset. (b) Transmission versus Si tip displacement in the z and y direction [see the dotted “scan line” in the inset of Fig. 4(a)], $\lambda_s = \lambda_{r,0}$.

After locating the field maxima at resonance in tapping mode, we placed the tip exactly in the middle of the largest maximum at the input side [labeled A in the inset of Fig. 4(a)], switched to contact mode, and measured the spectrum [Fig. 4(a)]. We found a full drop of about 7 dB in the transmitted power (black curve) for this cavity. After moving the tip to point B, we measured the spectrum again. The new spectrum (red), compared to the undisturbed one (blue) shows a shift in λ_r of about 2 nm and a reduction of Q by a factor of about 2, while the transmission has dropped by ~ 4 dB. To find the exact lateral dependence of the transmitted

power [in the y direction as shown by the dotted line in the inset of Fig. 4(a)] for a wavelength at $\lambda_{r,0}$, we plotted the transmitted power versus vertical tip displacement, see Fig. 4(b). The graph shows that the cavity resonance is highly sensitive to tip displacement and can be switched on and off by a lateral tip displacement of about 500 nm.

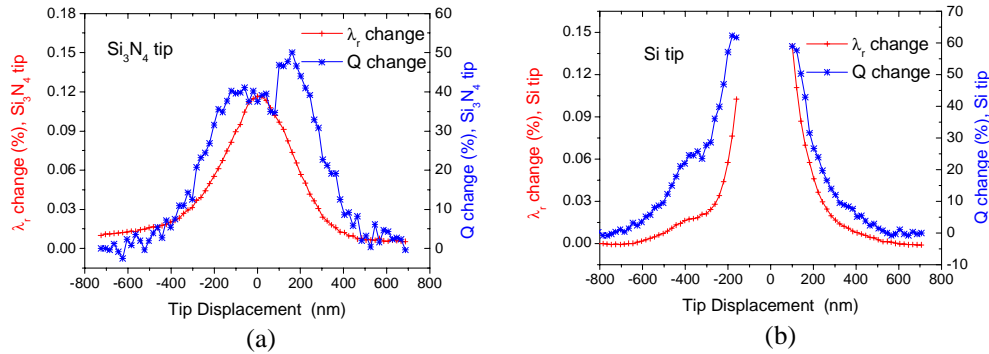


Fig. 5. Nano-mechanical tuning. (a) Change of Q and resonance wavelength detuning for a Si_3N_4 probe versus y -displacement along the scan line shown in Fig. 4(a). (b) The same but now for a Si tip. In close proximity to the field maximum no data could be obtained because the transmission had dropped below the noise level.

An even stronger effect can be obtained by vertical movement (z direction) of the probe, as was indicated by the tapping mode experiments shown in Figs. 3(d)-3(f). Full on/off switching can be achieved in only ~ 100 nm vertical displacement [blue curve in Fig. 4(b)]. The wavelength dependency of each point in the resonator could be found by performing 2D scans in the XY plane for wavelengths ranging from 1538 nm to 1544 nm with a step of 0.25 nm, using both a Si_3N_4 and an Si tip in contact mode. Using these results, fitted to the expected Lorentzian response, we mapped the shift of the resonance wavelength and the change in Q as a function of the displacement from the center position of the antinode. The results for the Si_3N_4 tip are shown in Fig. 5(a). A maximum detuning of λ_r by 1.8 nm (0.12 % of λ_s) is found together with a maximum Q change of 50 %. The shape of the Q -factor curve is less smooth due to the larger uncertainty in the width parameter found by applying the fitting procedure. The experiments with the Si tip show that a further detuning is possible [Fig. 5(b)]. However for tip positions too close to the field maximum, it was not possible to fit the data because the power had dropped below the noise level, as is also shown by the black curve in Fig. 4(a). We found a maximum detuning of λ_r by ~ 2.3 nm (0.15 % of λ_s) and a maximum change of Q by 65 %.

5. Conclusion

In conclusion, we have shown experimentally that an AFM probe can be used to map out the resonance pattern of a PhC MC with, to our knowledge, the highest resolution reported so far. The results show the exciting complex behavior that follows from the interaction of a nano-tip with the resonator mode, which is an interesting subject for future theoretical and experimental studies. Furthermore we have shown that the two important parameters (Q -factor and resonance wavelength) of a PhC MC can be nano-mechanically tuned over a considerable range. The results strongly motivate further exploitation of the tip-resonator mode interaction, which may be used for designing many new complex optical structures, such as a mechano-optically integrated reconfigurable PhC add-drop multiplexer. Another implication of our study is that near-field probing on high Q (or bandwidth limited ultra slow light [23]) structures cannot be performed without appreciably changing the optical properties of the device under study (while maintaining the same spatial resolution). Finally we mention that the strong advantage of this tuning is the ability to compensate for inevitable small

fabrication errors, i.e. shifting the resonance wavelengths or changing the Q-value to the desired values.

Acknowledgments

We thank Edwin Klein, Ronald Dekker and Frans Segerink for discussions and help. This work was supported by NanoNed, a national nanotechnology program coordinated by the Dutch ministry of Economic Affairs, and was also supported by the European Network of Excellence (ePIXnet).